Supramolecular Self-Assembly of Conjugated Diblock Copolymers

Hengbin Wang,[a] Wei You,[a] Ping Jiang,[a] Luping Yu,*[a] and H. Hau Wang[b]

Abstract: This paper describes the synthesis and characterization of a novel series of copolymers with different lengths of oligo(phenylene vinylene) (OPV) as the rod block, and poly(propylene oxide) as the coil block. Detailed characterization by means of transmission electron microscopy (TEM), atomic force microscopy (AFM), and small-angle neutron scattering (SANS) revealed the strong tendency of these copolymers to self-assemble into cylindrical micelles in solution and as-casted films on a nanometer scale. These micelles have a cylindrical OPV core surrounded by a poly(propylene glycol) (PPG) corona and readily align with each other to form parallel packed structures when mica is used as the substrate. A packing model has been proposed for these cylindrical micelles.

Keywords: conjugation · diblock copolymers · micelles · oligo(phenylene vinylene) · self-assembly

Introduction

Semicrystalline rod–coil block copolymers exhibit considerable morphological richness arising from the two forces that drive the microphase separation between the different blocks in the melt.[1–6] The dissimilarity of the two blocks favors the formation of segregated nanometer-scale domains (e.g., spheres, cylinders, lamellae), and crystallization of one block favors the formation of alternating amorphous and crystalline layers. Similarly, rod–coil block copolymers in a selective solvent could self-assemble into a variety of supramolecular structures through mutual interactions between polymer segments and solvent.[7–21] Conjugated polymers are rigid macromolecules and have been developed as advanced materials for photonic or electronic applications.[22–31] If the conjugated polymer chains can be organized into higher-order structures, novel functions at the molecular level may translate into solid-state bulk properties due to their unique π-electron system. Therefore, self-assembly of π-conjugated block copolymers constitutes a promising strategy for the construction of well-defined and stable nanometer-sized structures with chemical functionalities and physical properties that are of potential use in optoelectronic devices.[7–17,32,33] In our previous work we described the synthesis and phase-separation behavior of an oligo[(phenylene vinylene)-*co*-poly(ethylene glycol)], (OPV-PEG), system.[9] These diblock copolymers possess remarkable self-assembling abilities, forming long cylindrical micelles ($>1\,\mu m$). Transmission electron microscopy (TEM), atomic force microscopy (AFM), and small-angle neutron scattering (SANS) studies showed that the core of the micelles had a diameter of ~8–10 nm and was composed of OPV segments.

Since the PEGs with high-molecular weights are crystalline materials, the driving force for phase separation in OPV-PEG is high. In this paper we describe a new diblock-copolymer system consisting of a monodispersed rodlike conjugated oligo(phenylene vinylene), covalently bonded to a coil-like segment of poly(propylene glycol) (OPV-PPG). It was found that although the PPG is a less hydrophilic and amorphous material, the resulting copolymers still exhibit a strong driving force for phase separation. It was found that these copolymers could be aligned if a proper substrate was used. In this work we also discuss evidence of the fiber packing structures for both OPV-*co*-PEG and OPV-*co*-PPG copolymers.

Results and Discussion

Synthesis: These block copolymers were synthesized according to Scheme 1; the synthesis of the oligo(phenylene vinylene) building blocks is the same as previously reported.[9] This approach facilitates purification of the final block copolymers, and synthesis of triblock copolymers and other architectures. Three poly(propylene glycol) (PPG) polymers with molecular weights of 1000, 2500, and 4500 were used. The resulting copolymers were purified by column chromatography (silica gel) using an eluent mixture of chloroform/

[a] Dr. H. Wang, W. You, Dr. P. Jiang, Prof. L. Yu
Department of Chemistry and The James Franck Institute
University of Chicago, 5735 South Ellis Avenue
Chicago, IL 60637 (USA)
E-mail: lupingyu@midway.uchicago.edu

[b] Dr. H. H. Wang
Materials Science Division, Argonne National Laboratory
9700 South Cass Avenue, Argonne, IL 60439 (USA)

© 2004 Wiley-VCH Verlag GmbH & Co. KGaA, Weinheim
DOI: 10.1002/chem.200305554

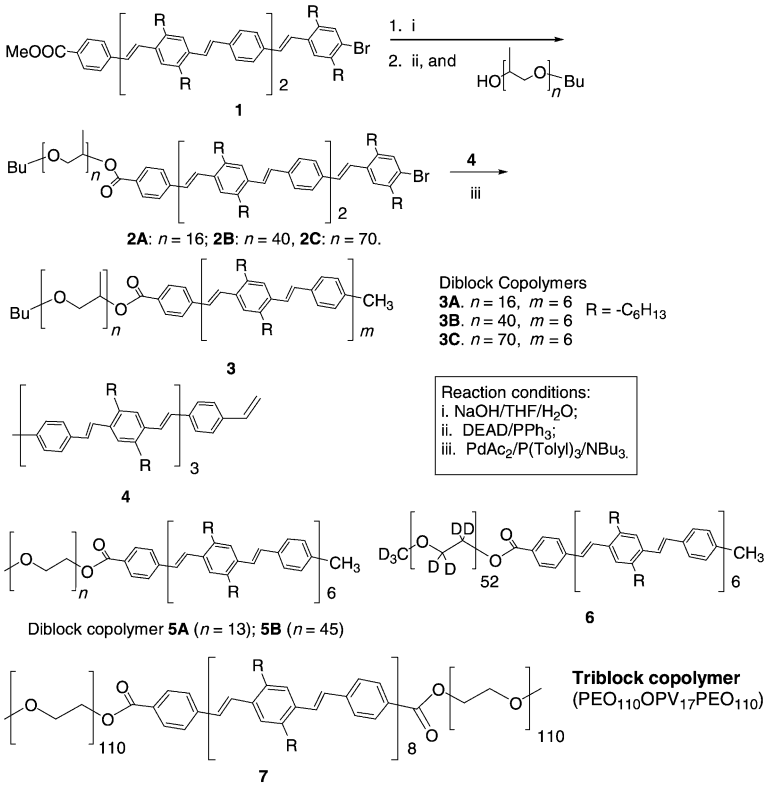

Scheme 1. Synthesis of OPV-PPG block copolymers.

methanol. All of the resulting block copolymers showed a narrow molecular-weight distribution with polydispersities of less than 1.1, as determined from gas-permeation chromatography (GPC). Mass spectrometry studies by means of MALDI–TOF measurements showed a close match between the calculated and experimental molecular weight (Figure 1). The chemical structures of these copolymers were confirmed by using ^{1}H NMR spectroscopy.

Phase separation behavior: Diluted solutions of these diblock copolymers, in mixed THF/H_2O or $CHCl_3$/CH_3OH solvents at various volume ratios, were used for the self-assembly studies. Water or methanol was used as the nonsolvent. Films cast from a solution (0.5 mg mL^{-1}) were studied by TEM and AFM under various conditions. Figure 2 shows the TEM image of copolymer **3C** (OPV_{13}-PPG_{70}) obtained when a carbon-coated copper grid was used as the substrate for the casting film. It shows that the whole film is composed of interwoven fibers with lengths of several thousand nanometers and diameters around 8–10 nm. These images were obtained without staining the sample. The widths of the fibers indicate that the dark fiber images are actually the core OPV part only (see below).

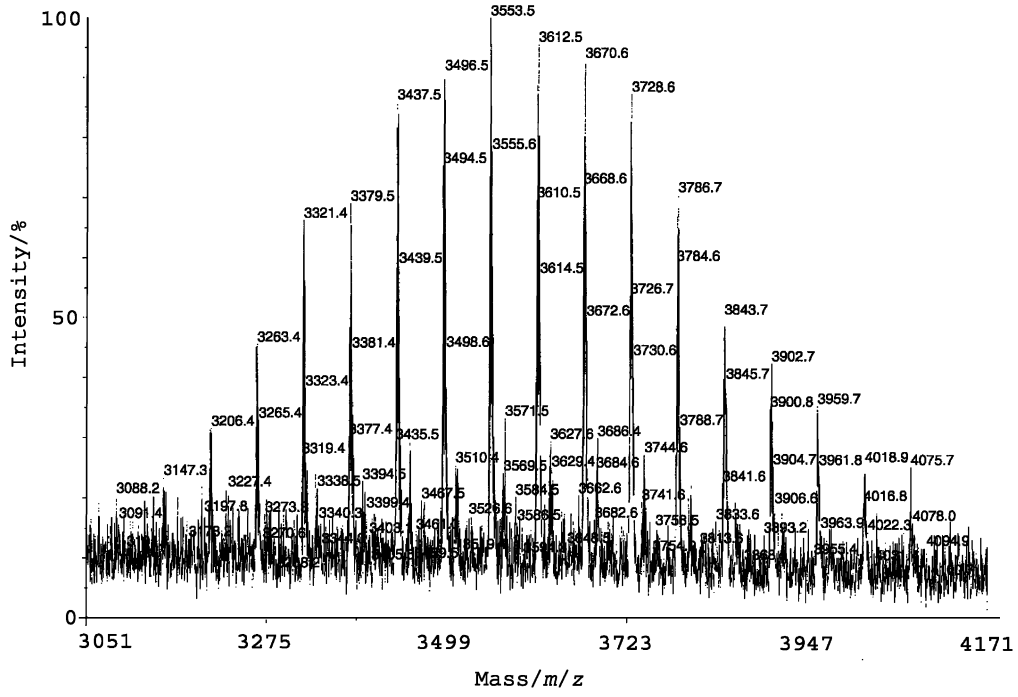

Figure 1. MS spectrum of copolymer **3A**.

 © 2004 Wiley-VCH Verlag GmbH & Co. KGaA, Weinheim

Figure 2. TEM image of copolymer **3C** on a carbon-coated copper grid.

SANS was used to study the self-assembly properties of OPV-PPG block copolymers in solution.[9] A very diluted solution (0.2 mg mL^{-1}) was used because the solubility of the OPV-PPG copolymer in [D_8]THF/D_2O is not as high as that of OPV-PEG copolymers that we studied previously.[9] Solutions of copolymers **3A** and **3C** were both studied; they have different lengths in PPG blocks and behave very differently from each other in SANS experiments. Figure 3 shows

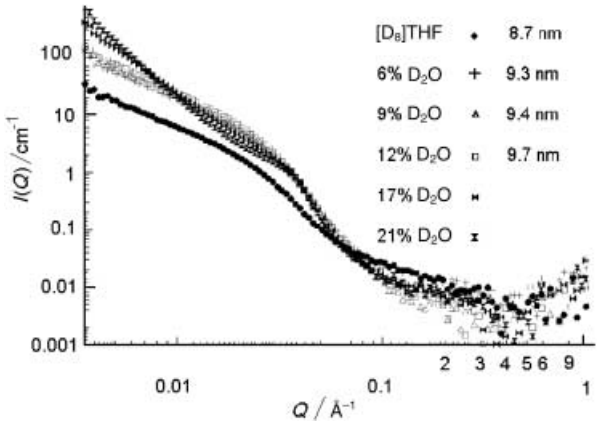

Figure 3. Small-angle neutron scattering curves of copolymer **3A** in [D_8]THF/D_2O mixed solvents (0%, 6%, 9%, 12%, 17%, and 21% D_2O) showing scattering intensity versus scattering vector.

the scattering intensities as a function of scattering vectors (Q) of copolymer **3A** (OPV_{13}-PPG_{16}) in [D_8]THF and [D_8]THF/D_2O mixed solvents. Modified Guinier analyses were carried out for both rodlike and spherical particles in the low Q region. The rodlike form factor clearly gave a much better fit (details for **3C** are given in Figure 5). The scattering curves show that copolymer **3A** scattered strongly and self-assembly occurred without D_2O present in the solution. A small amount of D_2O (6% w/w) doubled the scattering intensity. However, the increase was not as dramatic as in the OPV-PEG system. This indicates that the packing of the molecules inside the fibers is not so well organized. Continual increase of the D_2O/THF ratio from 6 to 12% gave only a slight increase in the scattering intensities. When a critical concentration of about 17% of D_2O was reached, a dramatic change in the scattering pattern was observed. The forward scattering intensity increased by about one order of magnitude. At the same time, a correlation peak appeared at a value of $Q=0.035$, which corresponded to the diameter of a swelled nanofiber (~18 nm) as described above. This means that the originally distinct rodlike aggregates condense into a phase of packed rods. The cross-sectional radii (R) calculated from modified Guinier analyses (with $Q_{max}R_c$ between 1.0 and 1.3) are also reported in Figure 3 and show that the radii of the fibers slightly increase with the addition of D_2O. The radius is only 8.7 nm when there is no D_2O present, which increases to 9.7 nm with 12% of D_2O. This implies water molecules swell the fibers. The results are consistent with the model that giant rodlike aggregates have a packed crystalline OPV core and a PPG shell.

In SANS experiments, the behavior of copolymer **3C**, with a long PPG block ($n=70$), was shown to be different from copolymer **3A**, with a short PPG block ($n=16$). We know that PPG will form the corona of the cylindrical micelles and determines the compatibility of the micelles with the solvent. With only 16 propylene oxide units in **3A**, the PPG block cannot cover the lateral fiber surface of the OPV block completely. In addition, the packing structure of **3A** is not very ordered. With the long-coil block of copolymer **3C**, the PPG blocks can protect the OPV block from unfavorable interaction with nonsolvent molecules and a well-defined packing structure can be expected. SANS results, as shown in Figure 4, indicate that **3C**, in pure [D_8]THF and in [D_8]THF with 3% D_2O, shows no micelle formation. However, when the D_2O/THF ratio was increased to 6% the scattering intensity increased by about one order of magnitude, which clearly indicated assembly. Modified Guinier analyses were carried out for the rodlike particles in the low Q region. The results for 6 and 12% D_2O/THF, with $Q_{max}R_c$ between 1.0 and 1.3, are shown in

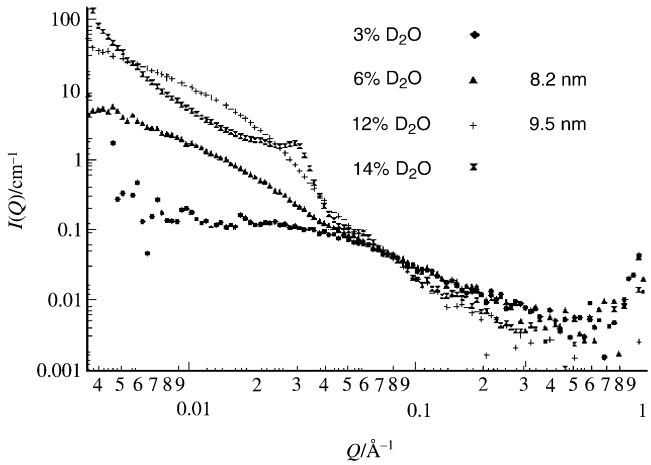

Figure 4. Small-angle neutron scattering curves of copolymer **3C** in [D_8]THF/D_2O mixed solvents (3%, 6%, 12%, and 14% D_2O) showing scattering intensity versus scattering vector.

© 2004 Wiley-VCH Verlag GmbH & Co. KGaA, Weinheim

Figure 5. The scattering intensity increased continuously when the D_2O ratio was increased, but the shape of the scattering pattern did not change before a critical concentration.

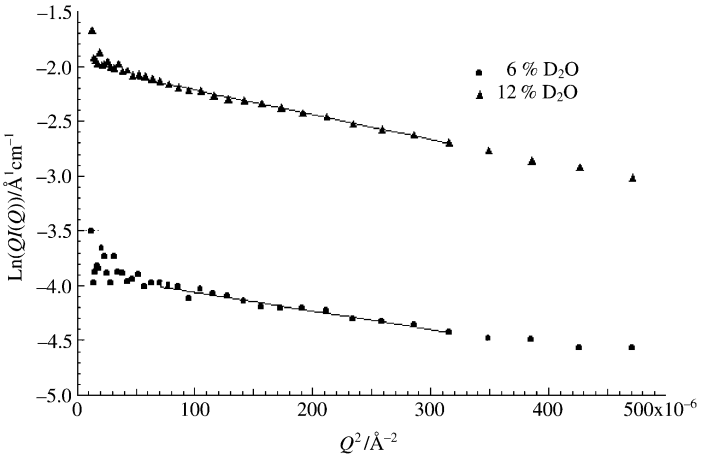

Figure 5. Modified Guinier analyses of **3C** for rodlike particles in 6 and 12% D_2O/THF in the low Q region.

This indicates that the fibers continuously swelled and no aggregation among fibers occurred. The calculated cross-sectional radii (R) slightly increased with the addition of D_2O. When a critical concentration of about 14% of D_2O was reached, a dramatic change in the scattering curve was observed. The forward-scattering intensity rises and at the same time a very sharp correlation peak appears at a Q value of 0.0294, corresponding to the distances between swelled nanofibers. This indicates again that the originally distinct rodlike aggregates condense into a phase of packed rods. Here we should point out that the correlation peak is much sharper than what appeared in the copolymer **3A** and **5** systems; this means the aggregate of fibers is more ordered. Figure 6 gives a schematic representation of the self-assembly of copolymer **3C** in solution with varying D_2O content.

The aggregate of fibers in solution was directly observed by fluorescence microscopy. The fibers gave a strong yellow fluorescence, which comes from the aggregated OPV block. Bundles of fibers are clearly observed at their critical water content (Figure 7). As expected, copolymer **3C** formed long and regular bundles and **3A** formed only short bundles.

Although cylindrical micelles were clearly observed by TEM and confirmed by SANS studies, what about the packing structure of the diblock molecules? This question was not explicitly answered in our previous work on OPV-PEG copolymers. Traditional micelle organization, with rigid head groups (OPV) on the outer layer and flexible coils (PPG or PEG) in the core, is not consistent with the TEM and SANS results, since the length of the conjugated block is about 8.5 nm, which corresponds to the diameter of the fiber measured from TEM studies. Based upon SANS and

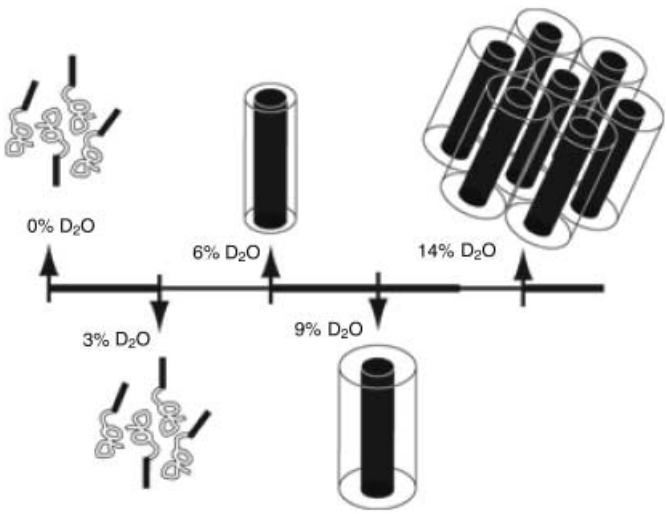

Figure 6. Schematic representation of the self-assembly of copolymer **3C** in solution.

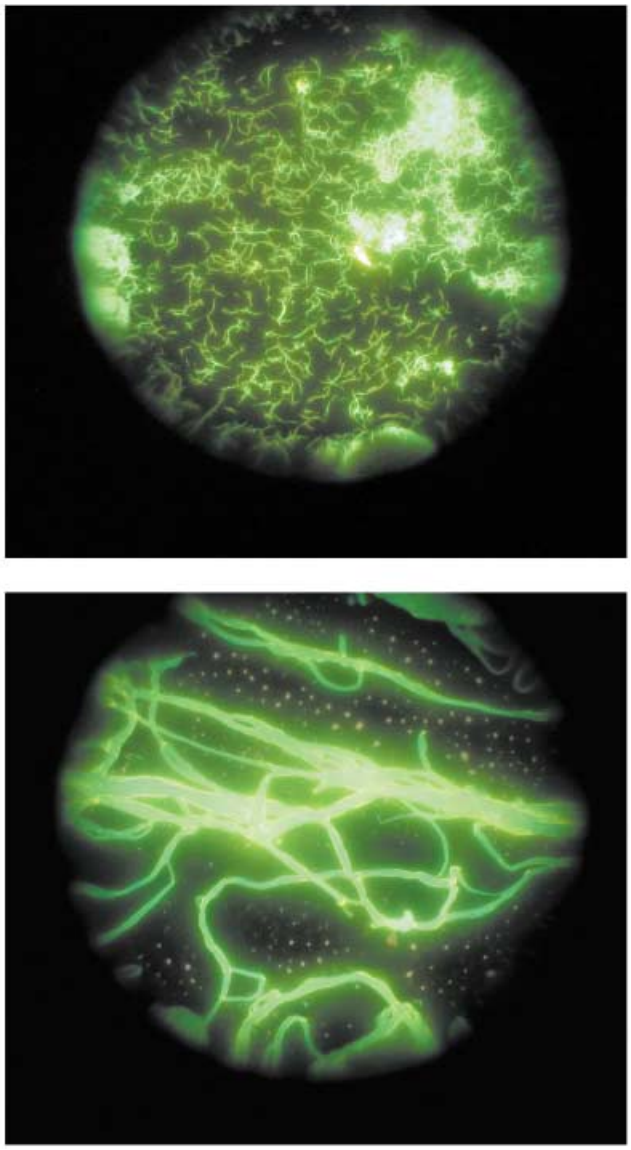

Figure 7. Fluorescence micrographs of copolymer **3A** (top) and **3C** (bottom) (×600).

 © 2004 Wiley-VCH Verlag GmbH & Co. KGaA, Weinheim

small-angle X-ray scattering (SAXS) studies, as well as our previous studies on OPV-PEG block copolymers, it is clear that the packing structures for these systems consist of a hydrophobic OPV inner core and a hydrophilic PEG or PPG outer shell. This model is also consistent with SANS results of copolymer **6**, in which the PEG block is fully deuterated. SANS measurements on OPV-[D]PEG in $[D_8]$THF gave a radius of 5.2 nm, roughly corresponding to the diameter of the OPV cores (10 nm).

Another important question is the arrangement of OPV segments inside the micelles. Two possible packing models are proposed in Figure 8 (monolayer above, bilayer below). Both packing models provide the same cross-sectional area. To differentiate between the two packing models, a PEG-OPV-PEG triblock copolymer was studied (copolymer **7**). TEM studies show this triblock copolymer forms similar cylindrical micelles, with a diameter of 10 nm, as did the diblock copolymers; this indicates they have the same kind of OPV core structure. In the SANS study with pure $[D_8]$THF or low water concentration no micelle formation was observed. This is because the triblock copolymer is more soluble in the solvent with two long PEG blocks at the outside. However, when 7% of water was added, the scattering intensity increased by one order of magnitude and the scattering curves fit the infinite-fiber model well, indicating micelle formation. By using the modified Guinier analysis for rod-like objects, a radius of 8.9 nm was obtained. Since it is unlikely for the triblock copolymer to form bilayer packing during the micelle formation, these results strongly suggest that the monolayer packing could be the more favored packing model for those block copolymers.

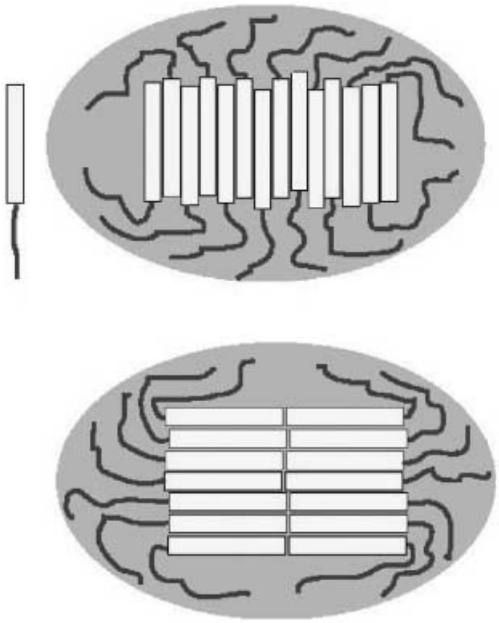

Figure 8. Schematic representation of two possible packing models (monolayer upper, bilayer lower) for OPV-PEO or OPV-PPO copolymers.

Preliminary alignment studies: Since the OPV-PPG diblock copolymers self-assemble into nanofibers, it is interesting to study their alignment on various substrates. Different substrates including polyimide, mica, and glass were studied. AFM images of copolymer **3C** showed the formation of long fibers on polyimide (Figure 9a). These fibers are randomly stacked; no alignment effect was observed. Compared to the TEM image of the copolymers, the diameters of these fibers are much larger; this means the fibers might aggregate together to form small bundles. Polyimide films rubbed with a Teflon bar were used as the substrate; no surface alignment was observed and random fibers were obtained. However, when mica was used as the substrate for copolymer **3C**, the fibers were aligned very well over a range as long as tens-of-micrometers without

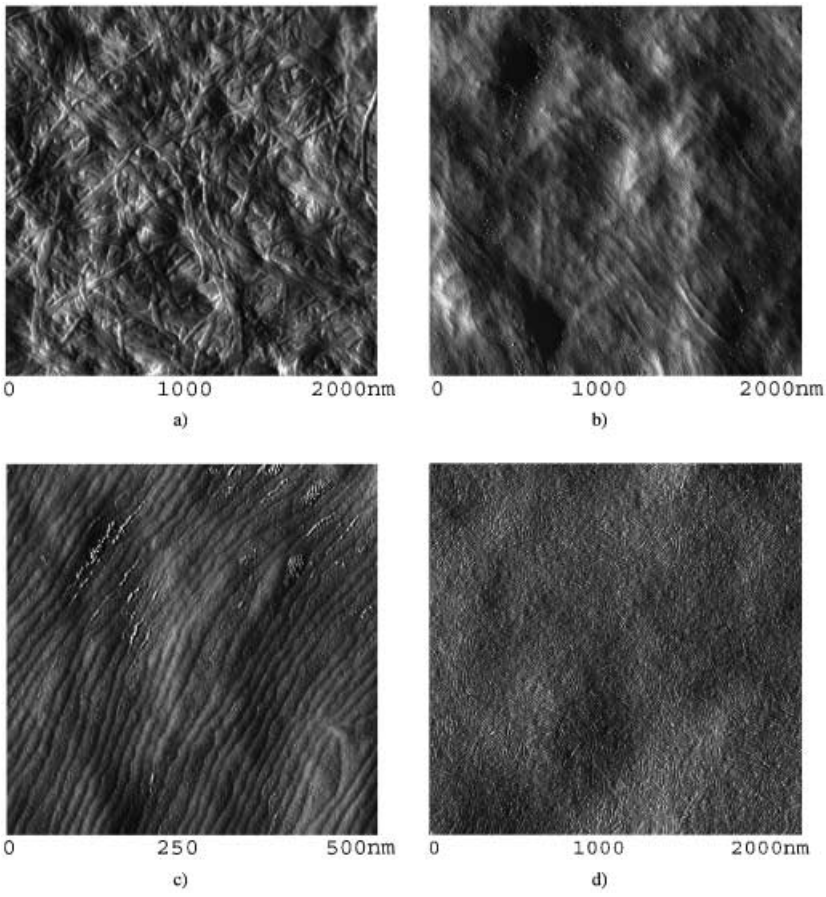

Figure 9. AFM images of copolymer a) **3C** on polyimide, b) and c) **3C** on mica, and d) **3A** on mica.

© 2004 Wiley-VCH Verlag GmbH & Co. KGaA, Weinheim

any special treatment (Figure 9b and c). The average diameter of the fibers was about 17 nm, which matches the SANS results of cylindrical micelles very well. It was also found that copolymer **3A** does not form a well-aligned structure on mica (Figure 9d).

These results indicate that both the substrate and the properties of coil blocks play important roles in the fiber alignment. Since the diblock copolymers exist in bundles of fibers, when the solvent evaporates or when the nonsolvent ratio increases to a critical content, interactions between PPG blocks and the surface will determine the orientation of the fibers. It is known that the surface dipoles of the newly cleaved mica exhibit a regular orientation and could have strong and directed interactions with the ether moieties in PPG.[34] The fiber bundles in copolymer **3C** are more organized and have more interacting ether sites than those in copolymer **3A**. The adhesion of the first layer of fiber bundles of copolymer **3C** is thus stronger than those of **3A**. After the first layer deposition, this layer plays the role of template to direct further orientation of fiber bundles. Shorter fiber lengths and less correlated bundles in copolymer **3A** are, therefore, responsible for less ordering of **3A** on the mica surface.

Thermotropic phase behavior: The OPV blocks, which have all-*trans* structures, are rigid rodlike molecules due to the delocalized π-conjugation. It is not surprising that all of the copolymers exhibit a reversible thermotropic liquid-crystalline phase. Differential scanning calorimetry (DSC) traces of the diblock copolymers indicated that the liquid-crystal isotropic transitions of three copolymers were at 223 °C, 212 °C, and 211 °C for **3A**, **3B**, and **3C**, respectively (Figure 10). Reversed transitions were observed from DSC traces of cooling scans at 210 °C, 200 °C, and 195 °C for copolymers **3A**, **3B**, and **3C**, respectively. Glass-transition temperatures of the copolymers were not observed and no melting peak of the PPG block was observed; this means that the PPG block is amorphous at room temperature. The values of the critical temperature (T_c) decreased as the size of the coil block increased. This is consistent with our previous studies of OPV-PEG block copolymers; a visible crystalline melting peak of an OPV block can be observed only for an OPV with 13 or more phenyl rings.[9] With the increase of the amorphous poly(propylene oxide) ratio, the melting temperature of the OPV block and the liquid-crystal isotropic transition decreased slightly. Polarized optical microscopic studies of these copolymers confirmed the liquid-crystal isotropic-phase transition temperature.

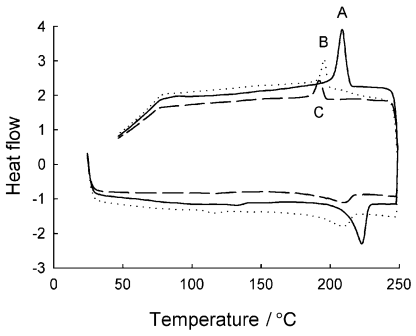

Figure 10. DSC traces of copolymer A) **3A**, B) **3B**, and C) **3C**.

Conclusion

A novel series of amphiphilic rod–coil copolymers with different lengths of oligo(phenylene vinylene) as the rod block and poly(propylene oxide) as the coil block were synthesized and characterized. These copolymers organize into cylindrical micelles in solution and as-cast films on a nanometer scale, as observed by using TEM, AFM, and SANS studies. These micelles have a cylindrical OPV core surrounded by a PPG corona. Based on the experimental results, a packing model was proposed for cylindrical micelles. It was found that the cylindrical micelles from copolymer **3C** readily aligned with each other to form parallel packed structures, especially when mica was used as the substrate.

Experimental Section

Materials: 1,4-Dichlorobenzene, 1-bromohexane, methyl 4-methyl benzoate, triethyl phosphite, poly(propylene oxide) methyl ether (average M_n ca. 1000, 2500, 4500, from Aldrich), and the other conventional reagents were used as received. Divinylbenzene was purified according to literature procedures.[8,9] Tetrahydrofuran was dried by distillation from sodium metal. Ethylene glycol dimethyl ether and *N,N*-dimethylformamide were dried by distillation from calcium hydride.

Techniques: ^{1}H NMR spectra were recorded in $CDCl_3$ on a Bruker AM500 spectrometer. Thermal analyses were performed on a Shimazu DSC-60 and TGA-50 under a nitrogen atmosphere at a heating rate of 10 °C min^{-1}. A Nikon Optiphoto-2 optical polarized microscope (magnification: ×400), equipped with a Creative Devices 50-600 high-temperature stage, was used to observe the thermal transitions and to analyze the anisotropic texture. Molecular-weight distributions were determined by using gel-permeation chromatography (GPC) with a Waters Associates liquid chromatograph equipped with a Waters 510 HPLC pump, Waters 410 differential refractometer, and Waters 486 tunable absorbance detector; THF was used as the solvent and polystyrene as the standard. Elemental analyses were performed by Atlantic Microlab. MALDI-TOF spectra were carried out in the Washington University Resource for Biomedical and Bio-organic Mass Spectrometry laboratory, with dithranol as the matrix. UV/Vis spectra were collected by using a Shimadzu UV-2401PC Recording Spectrophotometer. Emission Spectra were recorded using a Shimadzu RF-5301PC Spectrofluorophotometer.

Transmission electron microscopy: As-cast films were prepared by placing a drop of the copolymer solution onto carbon-coated or holey TEM grids. The grids were air-dried or dried in the atmosphere of the solvent. The specimen was examined in a Philips CM120 electron microscope operated at 120 kV.

Atomic force microscopy: The tapping mode AFM imaging of the sample was performed in air with a Multimode Nanoscope IIIA Scanning Probe Microscope (MMAFM, Digital Instruments). Cantilevers, with an Olympus Tapping Mode Etched Silicon Probe (Digital Instruments) with a nominal spring constant of 42 N m^{-1}, were used in the tapping mode with a type E scanner. The drive frequency was 270–350 kHz, and the drive amplitude was between 0.7 V and 1.1 V. The setpoint was usually around 0.6–0.9 of the free amplitude in our experiments. The pictures shown are height mode with a frame rate of 512.

Small-angle neutron scattering: Scattering experiments were performed by using the time-of-flight instrument SAND at the Intense Pulsed Neutron Source (IPNS) at Argonne National Laboratory. By using neutrons with wavelengths in the range of 0.5–14.0 Å by time-of-flight and a 40 × 40 cm^2 position sensitive proportional counter at a fixed sample-to-detec-

 © 2004 Wiley-VCH Verlag GmbH & Co. KGaA, Weinheim

tor distance of 2 m, SAND produced data in the scattering vector Q ($Q=4\pi\sin(\theta/\lambda)$, whereby θ is half the scattering angle and λ is the wavelength of the incident neutrons) of the range 0.004–0.8 $Å^{-1}$ in a single measurement. To obtain the best contrast for the SANS signals, deuterated THF was used as a solvent. In addition, D_2O was used for the investigation into the effect of water on the self-assembly of the diblock copolymer in deuterated THF. The solutions were measured in Suprasil (quartz) cylindrical cells with a 2 mm path length. The data for each sample were corrected for the backgrounds from the instrument, the Suprasil cell, solvent, and sample transmission. It was then placed on an absolute scale by using the routine procedures at IPNS.[10]

Synthesis: A general synthetic procedure is outlined in Scheme 1. Oligo(phenylene vinylene) segments were synthesized according to similar procedures described previously.[8,9]

Compound 2A: Compound **1** (0.8355 g, 0.679 mmol) and KOH (0.183 g, 3.4 mmol) were dissolved in THF (15 mL), and H_2O (0.6 mL) was added. The resulting solution was refluxed for 12 h and then poured into methanol (100 mL) at room temperature. The precipitate was collected by suction filtration and washed with methanol. The product was further purified by flash chromatography, using an eluent mixture of chloroform and methanol, to give a yellow solid (OPV6-acid). The mixture of poly(propylene oxide) monomethyl ether ($M_n=1000$) (0.33 g, 0.33 mmol), OPV6-acid (0.368 g, 0.3 mmol), and PPh_3 (87 mg, 0.33 mmol), in THF (15 mL), was heated to 80 °C. When all the starting material dissolved, it was cooled to 35 °C and diethyl azodicarboxylate (DEAD) (63 mg, 0.36 mmol) was added. The resulting solution was stirred at 35 °C for 24 h and then the DMF was removed by vacuum distillation. The product was further purified by flash chromatography, using an eluent mixture of chloroform and methanol, to give compound **2** as a yellow solid.

Compound 2A: ^{1}H NMR (500 MHz, $CDCl_3$): $\delta=8.06$ (d, $J=8$ Hz, 2H), 7.58 (d, $J=8$ Hz, 2H), 7.54–7.52 (m, 8H), 7.49–7.46 (m, 6H), 7.44 (s, 1H), 7.39 (d, $J=16$ Hz, 2H), 7.38 (d, $J=16$ Hz, 1H), 7.28 (d, $J=16$ Hz, 1H), 7.07 (d, $J=16$ Hz, 2H), 7.06 (d, $J=16$ Hz, 1H), 7.05 (d, $J=16$ Hz, 1H), 7.00 (d, $J=16$ Hz, 1H), 4.01 (d, $J=5.5$ Hz, 1H), 3.58–3.50 (m, 32H), 3.49–3.40 (m, 15H), 2.78 (m, 8H), 2.68 (m, 4H), 1.66 (m, 12H), 1.43 (m, 12H), 1.35 (m, 24H), 1.14 (m, 48H), 0.91 ppm (m, 18H); elemental analysis calcd (%) for $C_{135}H_{211}BrO_{18}$: C 73.63, H 9.66, Br 3.63; found: C 73.21, H 9.78.

Compound 2B: ^{1}H NMR (500 MHz, $CDCl_3$): $\delta=8.06$ (d, $J=8$ Hz, 2H), 7.58 (d, $J=8$ Hz, 2H), 7.54–7.52 (m, 8H), 7.49–7.46 (m, 6H), 7.44 (s, 1H), 7.39 (d, $J=16$ Hz, 2H), 7.38 (d, $J=16$ Hz, 1H), 7.28 (d, $J=16$ Hz, 1H), 7.07 (d, $J=16$ Hz, 2H), 7.06 (d, $J=16$ Hz, 1H), 7.05 (d, $J=16$ Hz, 1H), 7.00 (d, $J=16$ Hz, 1H), 4.01 (d, $J=5.5$ Hz, 1H), 3.58–3.50 (m, 80H), 3.49–3.40 (m, 40H), 2.78 (m, 8H), 2.68 (m, 4H), 1.66 (m, 12H), 1.43 (m, 12H), 1.35 (m, 24H), 1.14 (m, 120H), 0.91 ppm (m, 18H); elemental analysis calcd (%) for $C_{207}H_{355}BrO_{42}$: C 69.14, H 9.95, Br 2.22; found: C 68.72, H 10.05.

Compound 2C: ^{1}H NMR (500 MHz, $CDCl_3$): $\delta=8.06$ (d, $J=8$ Hz, 2H), 7.58 (d, $J=8$ Hz, 2H), 7.54–7.52 (m, 8H), 7.49–7.46 (m, 6H), 7.44 (s, 1H), 7.39 (d, $J=16$ Hz, 2H), 7.38 (d, $J=16$ Hz, 1H), 7.28 (d, $J=16$ Hz, 1H), 7.07 (d, $J=16$ Hz, 2H), 7.06 (d, $J=16$ Hz, 1H), 7.05 (d, $J=16$ Hz, 1H), 7.00 (d, $J=16$ Hz, 1H), 4.01 (d, $J=5.5$ Hz, 1H), 3.58–3.50 (m, 140H), 3.49–3.40 (m, 70H), 2.78 (m, 8H), 2.68 (m, 4H), 1.66 (m, 12H), 1.43 (m, 12H), 1.35 (m, 24H), 1.14 (m, 210H), 0.91 ppm (m, 18H); elemental analysis calcd (%) for $C_{297}H_{535}BrO_{72}$: C 66.83, H 10.10, Br 1.50; found: C 66.23, H 10.35.

Compound 3A: ^{1}H NMR (500 MHz, $CDCl_3$): $\delta=8.04$ (d, $J=8$ Hz, 2H), 7.58–7.52 (m, 21H), 7.47–7.37 (m, 26H), 7.32 (d, $J=16$ Hz, 2H), 7.19 (d, $J=8$ Hz, 2H), 7.06 (d, $J=16$ Hz, 10H), 7.03 (d, $J=16$ Hz, 1H), 4.01 (d, $J=5.5$ Hz, 1H), 3.58–3.50 (m, 32H), 3.49–3.40 (m, 15H), 2.78 (m, 12H), 2.38 (s, 3H), 1.66 (m, 12H), 1.43 (m, 12H), 1.35 (m, 24H), 1.14 (m, 48H), 0.91 ppm (m, 18H); elemental analysis calcd (%) for $C_{228}H_{328}O_{18}$: C 81.57, H 9.85; found: C 81.32, H 9.96.

Compound 3B: ^{1}H NMR (500 MHz, $CDCl_3$): $\delta=8.04$ (d, $J=8$ Hz, 2H), 7.58–7.52 (m, 21H), 7.47–7.37 (m, 26H), 7.31 (d, $J=16$ Hz, 2H), 7.19 (d, $J=8$ Hz, 2H), 7.06 (d, $J=16$ Hz, 10H), 7.04 (d, $J=16$ Hz, 1H), 4.01 (d, $J=5.5$ Hz, 1H), 3.58–3.50 (m, 80H), 3.49–3.40 (m, 40H), 2.78 (m, 12H), 2.37 (s, 3H), 1.66 (m, 12H), 1.43 (m, 12H), 1.35 (m, 24H), 1.14 (m, 120H), 0.91 ppm (m, 18H); elemental analysis calcd (%) for $C_{300}H_{472}O_{42}$: C 75.84, H 10.01; found: C 75.62, H 10.34.

Compound 3C: ^{1}H NMR (500 MHz, $CDCl_3$): $\delta=8.05$ (d, $J=8$ Hz, 2H), 7.58–7.52 (m, 21H), 7.47–7.37 (m, 26H), 7.31 (d, $J=16$ Hz, 2H), 7.19 (d, $J=8$ Hz, 2H), 7.06 (d, $J=16$ Hz, 10H), 7.03 (d, $J=16$ Hz, 1H), 4.01 (d, $J=5.5$ Hz, 1H), 3.58–3.50 (m, 140H), 3.49–3.40 (m, 70H), 2.78 (m, 12H), 2.38 (s, 3H), 1.66 (m, 12H), 1.43 (m, 12H), 1.35 (m, 24H), 1.14 (m, 210H), 0.91 ppm (m, 18H); elemental analysis calcd (%) for $C_{390}H_{652}O_{72}$: C 72.14, H 10.12; found: C 72.01, H 10.25.

Acknowledgement

We gratefully acknowledge the financial support of the National Science Foundation, AFOSR, and the NSF MRSEC program at the University of Chicago. Partial support was also provided by the UC-Argonne Nanoscience consortium and The Petroleum Research Fund, administered by the ACS. Work at Argonne National Laboratory is sponsored by the U.S. Department of Energy, Office of Basic Energy Science, Division of Materials Science, under Contract W-31-109-ENG-38. H.H. Wang acknowledges support from DOE S&P center, Smart Structures based on Electroactive Polymers, and the use of the ANL/IPNS facility.

[1] D. R. M. Williams, G. H. Fredrickson, *Macromolecules* **1992**, *25*, 3561.
[2] J. L. Radzilowsk, S. I. Stupp, *Macromolecules* **1994**, *27*, 7747.
[3] G. Widawski, M. Rawiso, B. Francois, *Nature* **1994**, *369*, 387.
[4] S. I. Stupp, V. Lebonheur, K. Walker, L. S. Li, K. E. Huggins, M. Keser, A. Amstutz, *Science* **1997**, *276*, 384.
[5] M. Lee, B.-K. Cho, H. Kim, W.-C. Zin, *Angew. Chem.* **1998**, *110*, 661; *Angew. Chem. Int. Ed.* **1998**, *37*, 638.
[6] J. T. Chen, E. L. Thomas, C. K. Ober, G. Mao, *Science* **1996**, *273*, 343.
[7] W. J. Li, L. P. Yu, *Macromolecules* **1996**, *29*, 7329, .
[8] W. Li, H. Wang, L. Yu, T. L. Morkved, H. M. Jaeger, *Macromolecules* **1999**, *32*, 3034.
[9] H. B. Wang, H. Wang, V. S. Urban, P. Thiyagarajan, K. C. Littrell, L. P. Yu, *J. Am. Chem. Soc.* **2000**, *122*, 6855.
[10] V. Urban, H. H. Wang, P. Thiyagarajan, K. C. Littrell, H. B. Wang, L. Yu, *J. Appl. Crystallogr.* **2000**, *33*, 645.
[11] J. Massey, K. N. Power, I. Manners, M. A. Winnik, *J. Am. Chem. Soc.* **1998**, *120*, 9533.
[12] S. A. Jenekhe, X. L. Chen, *Science* **1998**, *279*, 1903.
[13] M. A. Hempenius, B. M. W. Langeveld-Voss, J. A. E. H. van Haare, R. A. J. Janssen, S. S. Sheiko, J. P. Spatz, M. Möller, E. W. Meijer, *J. Am. Chem. Soc.* **1998**, *120*, 2798.
[14] P. Leclère, A. Calderone, D. Marsitzky, V. Francke, Y. Geerts, K. Müllen, J. L. Brédas, R. Lazzaroni, *Adv. Mater.* **2000**, *12*, 1042.
[15] G. N. Tew, M. U. Pralle, S. I. Stupp, *J. Am. Chem. Soc.* **1999**, *121*, 9852.
[16] U. Stalmach, B. de Boer, C. Videlot, P. F. van Hutten, G. Hadziioannou, *J. Am. Chem. Soc.* **2000**, *122*, 5464.
[17] M. Lee, Y.-S. Jeong, B.-K. Cho, N.-K. Oh, W.-C. Zin, *Chem. Eur. J.* **2002**, *8*, 876.
[18] J. T. Chen, E. L. Thomas, C. K. Ober, S. S. Hwang, *Macromolecules* **1995**, *28*, 1688.
[19] Y. Tu, X. Wan, D. Zhang, Q. Zhou, C. Wu, *J. Am. Chem. Soc.* **2000**, *122*, 10201.
[20] J. L. Radzilowsk, B. O. Carragher, S. I. Stupp, *Macromolecules* **1997**, *30*, 2110.
[21] S. I. Stupp, V. Lebonheur, K. Walker, L. S. Li, K. E. Huggins, M. Keser, A. Amstutz, *Science* **1997**, *276*, 384.
[22] N. C. Greenham, S. C. Moratti, D. D. C. Bradley, R. H. Friend, A. B. Holmes, *Nature* **1993**, *365*, 628.
[23] D. Braun, A. J. Heeger, *Appl. Phys. Lett.* **1991**, 58, 1982.
[24] F. Hide, M. A. Diazgarcia, B. J. Schwartz, M. R. Anderson, Q. B. Pei, A. J. Heeger, *Science* **1996**, *273*, 1833.
[25] H. Sirringhaus, N. Tessler, R. H. Friend, *Science* **1998**, *280*, 1741.
[26] T. Cassagneau, F. Caruso, *Adv. Mater.* **2002**, *14*, 1837.
[27] J. W. Hong, B. S. Gaylord, G. C. Bazan, *J. Am. Chem. Soc.* **2002**, *124*, 11868.

© 2004 Wiley-VCH Verlag GmbH & Co. KGaA, Weinheim

[28] L. Schmidt-Mende, A. Fechtenkötter, K. Müllen, E. Moons, R. H. Friend, J. D. MacKenzie, *Science* **2001**, *293*, 1119.
[29] W. U. Huynh, J. J. Dittmer, A. P. Alivisatos, *Science* **2002**, *295*, 2425.
[30] Z. G. Zhu, T. M. Swager, *J. Am. Chem. Soc.* **2002**, *124*, 9670.
[31] W. Lu, A. G. Fadeev, B. H. Qi, E. Smela, B. R. Mattes, J. Ding, G. M. Spinks, J. Mazurkiewicz, D. Z. Zhou, G. G. Wallace, D. R. MacFarlane, S. A. Forsyth, M. Forsyth, *Science* **2002**, *297*, 983.
[32] P. Leclère, E. Hennebicq, A. Calderone, P. Brocorens, A. C. Grimsdale, K. Mullen, J. L. Brédas, R. Lazzaroni, *Prog. Polym. Sci.* **2003**, *28*, 55.
[33] H. B. Wang, M.-K. Ng, L. P. Yu, B. H. Lin, M. Meron, Y. N. Xiao, *Chem. Eur. J.* **2002**, *8*, 3246 – 3253.
[34] F. Balzer, H.-G. Rubahn, *Surf. Sci.* **2002**, *507*–510, 588.

Received: September 19, 2003 [F5554]

 © 2004 Wiley-VCH Verlag GmbH & Co. KGaA, Weinheim